

Influence of cloud feedback on annual variation of global mean surface temperature

Yoko Tsushima and Syukuro Manabe

Frontier Research System for Global Change, Kanagawa, Japan

Abstract. The goal of this study is to estimate the cloud radiative feedback effect on the annual variation of the global mean surface temperature using radiative flux data from the Earth Radiation Budget Experiment. We found that the influence of the cloud feedback upon the change of the global mean surface temperature is quite small, though the increase of the temperature is as much as 3.3 K from January to July. On a global scale, we found no significant relationship between either solar reflectivity of clouds or effective cloud top height and the annual cycle of surface temperature. The same analysis was repeated using the output from three general circulation models, which explicitly predict microphysical properties of cloud cover. On a global scale, both solar cloud reflectivity and cloud top height increase significantly with the increase of surface temperature, in contrast to the observation. The comparative analysis conducted here could be used as an effective test for evaluating the cloud feedback process of a model.

1. Introduction

The heat balance of this planet is maintained by the heating due to the absorption of incoming solar radiation and the cooling due to the emission of outgoing radiation. It is well known that cloud cover exerts a large influence on the Earth's heat budget. For example, clouds reflect solar radiation thereby cooling the atmosphere-Earth surface system. Clouds also absorb the upward infrared radiation emitted from the Earth's surface and lower troposphere with relatively high temperature and emits it at low temperature, reducing the outgoing radiation from the top of the atmosphere. Thus clouds also have a warming effect (i.e., the greenhouse effect). Since the cooling effect usually exceeds the warming effect [e.g., *Manabe and Wetherald, 1967*], cloud cover has a net cooling effect upon the heat balance [e.g., *Ramanathan et al., 1989*].

It has been speculated that accompanying with climate change such as global warming, the distribution and optical properties of clouds are altered, significantly affecting the temperature change in the atmosphere-Earth surface system. This is called the cloud feedback effect. Unfortunately, our current knowledge of the cloud feedback effect is far from satisfactory. We do not know the sign let alone the magnitude of the effect. The large range of uncertainty associated with the estimate of future climate change by the Intergovernmental Panel on Climate Change is attributable in no small part to our failure to reliably determine the influ-

ence of the cloud feedback effect upon global warming.

In order to reliably project future climate change, it is therefore necessary to validate the cloud feedback process of a general circulation model (GCM) of the atmosphere based upon observation. In this study, we want to test the cloud feedback effect of a model by quantitatively comparing the observed and simulated cloud feedback effect upon the annual variation of global mean surface temperature. Unfortunately, as described below, the pattern of observed annual variations of global mean surface air temperature is highly variable horizontally and is quite different from the pattern of global warming simulated by a model. Therefore there is no guarantee that the cloud feedback process affects the annual variation of global mean surface temperature in the same way as it affects the increase of surface temperature associated with global warming. Nevertheless, the annual variation of surface temperature is the largest observable climate change available for validating of a climate model. In the present study, we quantitatively evaluate the influence of the cloud feedback process upon the annual variation of global mean surface temperature, using the observed solar and long-wave fluxes at the top of the atmosphere. We chose the global domain for the analysis because global averaging eliminates the undue influence of local change in radiative fluxes due to horizontal movement of cloud cover.

Figure 1a illustrates the annual variations of surface air temperature averaged over the entire globe and the Northern and Southern Hemispheres. It shows that surface temperature averaged over the Northern Hemisphere has an annual variation that is out of phase and is much larger than that of the Southern Hemispheres.

Copyright 2001 by the American Geophysical Union.

Paper number 2000JD000235.
0148-0227/01/2000JD000235\$09.00

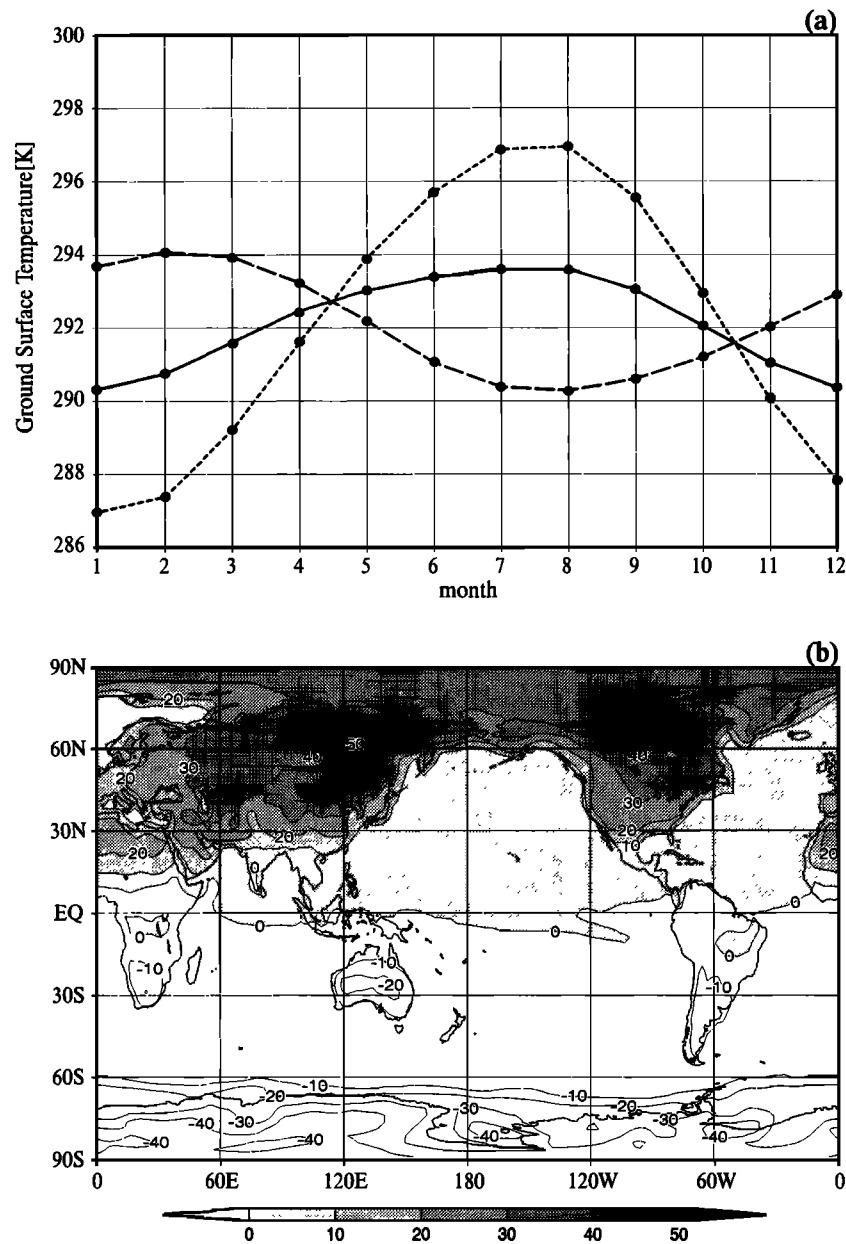


Figure 1. (a) Annual variation of surface temperature (K). Long dash, short dash, and solid line denote Southern Hemisphere, Northern Hemisphere, and global mean value. (b) Geographical distribution of the difference in monthly mean surface temperature between July and January. Contour intervals are 10 K.

Thus global mean surface temperature varies in phase with Northern Hemisphere mean surface temperature and has an annual range of about 3.3 K. This is because the annual range of the surface temperature is much larger over continents than over oceans and the fraction of continents is larger in the Northern than in the Southern Hemisphere. Although the annual range of surface temperature (Figure 1b) has quite different geographical distribution from the simulated response of surface temperature to the doubling of atmospheric carbon dioxide, the global mean value of the former is comparable in magnitude to the latter. The main goal

of the present study is to evaluate and compare the observed and simulated influences of the cloud feedback effect upon the annual variation of the global mean surface temperature.

In section 2, the basic formulation is obtained for analyzing the cloud feedback process, and the data used for the analysis are identified. Section 3 analyzes the cloud feedback process in the annual variation of global mean surface temperature, using radiative fluxes observed at the top of the atmosphere. Section 4 compares the results thus obtained with those from three general circulation models of the atmosphere, in which cloud

microphysical properties are parameterized explicitly. Finally, the implication of the results obtained is discussed in section 5.

2. Feedback Parameter

2.1. Basic Equations

This subsection derives the basic formulation used for analyzing the cloud feedback process in the annual variation of the global mean temperature. Normally, feedback analysis is applied to the equilibrium response of the global mean surface temperature to radiative forcing such as the change in the atmospheric concentration of greenhouse gases. In the present study, however, it is applied to the annual variation of global mean surface temperature, which is the periodic response to the seasonal variation of solar radiation.

The global mean, net downward flux of radiation at the top of the atmosphere R may be subdivided as

$$\overline{R} = \overline{R_S} + \overline{R_L}, \quad (1)$$

where R_S and R_L are the net downward fluxes of solar and terrestrial radiation, respectively, at the top of the atmosphere. Here $\overline{(\quad)}$ indicates global averaging of the variable (\quad) . (In this study, the area-averaging $\overline{(\quad)}$ is made over the area between 60°N and 60°S as explained in subsection 2.3.) $\overline{R_S}$ and $\overline{R_L}$ may be expressed as

$$\overline{R_S} = \overline{S_0(1 - \alpha)}, \quad (2)$$

and

$$\overline{R_L} = -\overline{L}, \quad (3)$$

where α is the planetary albedo (i.e., the reflectivity of incoming solar radiation), S_0 is the flux of incoming solar radiation, and L is the upward flux of terrestrial radiation at the top of the atmosphere.

In the annual variation, the differential of radiative flux at the top of the atmosphere may be subdivided as

$$d\overline{R} = \frac{\partial \overline{R_S}}{\partial S_0} dS_0 - \lambda d\overline{T_s}, \quad (4)$$

where λ is the feedback parameter [e.g., Dickinson, 1981] and $\overline{T_s}$ denotes the global mean surface temperature. The first term on the right-hand side of (4) indicates the contribution from the change in the incoming solar flux at the top of the atmosphere. The second term indicates the change in radiative flux associated with an infinitesimal change of the global mean surface temperature $d\overline{T_s}$, which results from the annual variation of solar insolation. Following Wetherald and Manabe [1988], the feedback parameter λ may be expressed by

$$\lambda = - \left(\overbrace{\frac{\partial R}{\partial T} \frac{dT}{d\overline{T_s}}} + \overbrace{\frac{\partial R}{\partial r} \frac{dr}{d\overline{T_s}}} + \overbrace{\frac{\partial R}{\partial C} \frac{dC}{d\overline{T_s}}} + \overbrace{\frac{\partial R}{\partial a} \frac{da}{d\overline{T_s}}} \right), \quad (5)$$

where

$$\overbrace{(\quad)} \equiv \int_0^{p_s} (\quad) \frac{dp}{g}. \quad (6)$$

Here p denotes pressure, p_s is surface pressure, and g is the acceleration of gravity. The four terms on the right-hand side of (5) represent the contributions from the changes in temperature T , mixing ratio of water vapor r , cloud cover C , and surface albedo a .

The feedback effect may be divided into basic radiative damping of surface temperature anomalies and the modification of the radiative damping through other feedback processes. The outgoing flux of terrestrial radiation at the top of the atmosphere follows the so called Stefan-Boltzmann law and is related to the global mean surface temperature as

$$\overline{R_L} = -\overline{L} \equiv -\varepsilon \sigma \overline{T_s}^4, \quad (7)$$

where σ is the Stefan-Boltzmann coefficient and ε is a coefficient of planetary emission. Using (7), the first term on the right-hand side of (5) may be expressed as

$$\begin{aligned} \overbrace{\frac{\partial R}{\partial T} \frac{dT}{d\overline{T_s}}} &= \overbrace{\frac{\partial R_L}{\partial T} \frac{dT}{d\overline{T_s}}} \\ &= -\lambda_0 + \overbrace{\frac{\partial R_L}{\partial(T - \overline{T_s})} \frac{d(T - \overline{T_s})}{d\overline{T_s}}}, \end{aligned} \quad (8)$$

where

$$\lambda_0 = 4\varepsilon \sigma \overline{T_s}^3, \quad (9)$$

representing the strength of the basic Stefan-Boltzmann radiative damping. The second term on the right-hand side of (8) is the net downward flux change associated with the change in the lapse rate profile. Using (8), one can rewrite (5) as follows:

$$\lambda = \lambda_0(1 - f_{LR} - f_r - f_C - f_a), \quad (10)$$

where

$$\begin{pmatrix} f_{LR} \\ f_r \\ f_C \\ f_a \end{pmatrix} = \frac{1}{\lambda_0} \begin{pmatrix} \overbrace{\frac{\partial R}{\partial(T - \overline{T_s})} \frac{d(T - \overline{T_s})}{d\overline{T_s}}} \\ \overbrace{\frac{\partial R}{\partial r} \frac{dr}{d\overline{T_s}}} \\ \overbrace{\frac{\partial R}{\partial C} \frac{dC}{d\overline{T_s}}} \\ \overbrace{\frac{\partial R}{\partial a} \frac{da}{d\overline{T_s}}} \end{pmatrix}. \quad (11)$$

Parameters f_{LR} , f_r , f_C , and f_a represent the relative magnitude of the modification to the basic feedback effect of Stefan-Boltzmann radiative damping through the changes in lapse rate, mixing ratio of water vapor,

cloud cover, and surface albedo. They are called gain factors and used by *Hansen et al.* [1984] to evaluate the contribution of various feedback effects in their climate model. As (10) indicates, a positive gain factor contributes to the reduction of λ , for example, exerting positive feedback upon the change of surface temperature. The gain factor for the cloud feedback processes f_C may be subdivided into solar and longwave components as follows:

$$f_C = f_{CS} + f_{CL}, \quad (12)$$

where

$$(f_{CS}, f_{CL}) \equiv \frac{1}{\lambda_0} \left[\overbrace{\frac{\partial R_S}{\partial C} \frac{dC}{dT_s}}^{\text{---}}, \overbrace{\frac{\partial R_L}{\partial C} \frac{dC}{dT_s}}^{\text{---}} \right]. \quad (13)$$

As discussed in subsection 2.2 on cloud forcing, the cloud gain factors f_{CS} and f_{CL} are computed from (13).

2.2. Cloud Forcing

This subsection derives the formula for estimating the cloud gain factors f_{CS} and f_{CL} defined in subsection 2.1. Following *Charlock and Ramanathan* [1985], solar and longwave cloud forcings are defined as

$$CF_S \equiv R_S - R_{S0} \quad (14)$$

and

$$CF_L \equiv R_L - R_{L0}, \quad (15)$$

where R_{S0} and R_{L0} are the net downward fluxes of solar and terrestrial radiation at the top of cloud-free atmosphere, respectively. Since $\partial(CF_S)/\partial C = \partial(R_S)/\partial C$ and $\partial(CF_L)/\partial C = \partial(R_L)/\partial C$, (13) may be rewritten as follows:

$$(f_{CS}, f_{CL}) = \left(\frac{1}{\lambda_0} \overbrace{\frac{\partial CF_S}{\partial C} \frac{dC}{dT_s}}^{\text{---}}, \frac{1}{\lambda_0} \overbrace{\frac{\partial CF_L}{\partial C} \frac{dC}{dT_s}}^{\text{---}} \right). \quad (16)$$

Here we shall obtain the relationship necessary to compute the gain factor of cloud feedback from the annual variation of solar and longwave cloud forcing. Using (2) and (14), solar cloud forcing (CF_S) may be expressed as

$$CF_S = S_0(\alpha_0 - \alpha), \quad (17)$$

where α_0 is the planetary albedo for clear sky. For convenience of analysis, we introduce the "annually normalized solar cloud forcing" (CF_{SA}), defined by

$$CF_{SA} = [S_0]^A (\alpha_0 - \alpha), \quad (18)$$

where

$$[(\)]^A = \left(\int^{\text{1 year}} (\) dt \right) / (1 \text{ year}). \quad (19)$$

The total derivatives of annually normalized solar cloud forcing and longwave cloud forcing with respect to the global mean surface temperature may be expressed by the following equations:

$$\frac{dCF_{SA}}{dT_s} = \overbrace{\frac{\partial CF_{SA}}{\partial C} \frac{dC}{dT_s}}^{\text{---}} + \overbrace{\frac{\partial CF_{SA}}{\partial r} \frac{dr}{dT_s}}^{\text{---}} + \overbrace{\frac{\partial CF_{SA}}{\partial a} \frac{da}{dT_s}}^{\text{---}} \quad (20)$$

$$\frac{dCF_L}{dT_s} = \overbrace{\frac{\partial CF_L}{\partial C} \frac{dC}{dT_s}}^{\text{---}} + \overbrace{\frac{\partial CF_L}{\partial r} \frac{dr}{dT_s}}^{\text{---}} + \overbrace{\frac{\partial CF_L}{\partial T} \frac{dT}{dT_s}}^{\text{---}}. \quad (21)$$

Using an algorithm for computing atmospheric radiative transfer, we estimated the magnitudes of the second and third terms in (20) and (21) and found that they are small (see appendix A). Neglecting the second and third terms on the right-hand sides of (20) and (21), one gets the following approximate relationship:

$$\frac{dCF_{SA}}{dT_s} \simeq \overbrace{\frac{\partial CF_{SA}}{\partial C} \frac{dC}{dT_s}}^{\text{---}} \quad (22)$$

$$\frac{dCF_L}{dT_s} \simeq \overbrace{\frac{\partial CF_L}{\partial C} \frac{dC}{dT_s}}^{\text{---}}. \quad (23)$$

Using the relationship

$$\frac{\partial CF_{SA}}{\partial C} = \left[\frac{\partial CF_S}{\partial C} \right]_{S_0=\overline{S_0}^A}, \quad (24)$$

(16) may be rewritten as

$$([f_{CS}]_{S_0=\overline{S_0}^A}, f_{CL}) \simeq \left(\frac{1}{\lambda_0} \overbrace{\frac{dCF_{SA}}{dT_s}}^{\text{---}}, \frac{1}{\lambda_0} \overbrace{\frac{dCF_L}{dT_s}}^{\text{---}} \right). \quad (25)$$

From (13) and (25), cloud gain factor f_C may be represented by

$$f_C = f_{CS} + f_{CL} = \frac{1}{\lambda_0} \overbrace{\frac{d(CF_{SA} + CF_L)}{dT_s}}^{\text{---}}. \quad (26)$$

In the present study, the gain factors f_{CS} , f_{CL} , and f_C defined above are estimated using (25) and (26).

2.3. Data

Solar and longwave cloud forcing, which are used for the feedback analysis described in this study, are computed from the data of monthly mean radiative fluxes at the top of the atmosphere. The data were obtained by *Harrison et al.* [1990] for February 1985 to February 1990, using the data from the Earth Radiation Budget Experiments (ERBE).

Monthly mean surface temperature needed for the analysis is obtained from the National Center for En-

vironmental Prediction (NCEP)/National Center for Atmospheric Research (NCAR) reanalysis [Kalnay *et al.*, 1996], covering January 1982 to December 1994. Monthly mean total cloudiness is determined using the D2 data from the International Cloud Climatology Project (ISCCP) that are available from January 1986 to January 1987 and December 1987 to February 1993.

The monthly climatologies of radiative fluxes, surface temperature, and total cloudiness are obtained by averaging monthly mean grid point data over 5-, 12-, and 6-year periods, respectively. The monthly mean radiative flux data for clear sky needed for computing cloud radiative forcing have large regions where the data are sporadically missing. For these regions, monthly mean clear sky fluxes were computed averaging over only those years when ERBE data were available. Fortunately, solar and longwave radiation fluxes for clear sky are available in 88% of the analysis domain identified in next paragraph.

Because of the difficulty in reliably determining solar cloud forcing over polar regions covered by snow, sea ice, and/or continental ice sheets with high surface albedo as noted by Nemesure *et al.* [1994], the analysis was conducted over the domain bounded by 60°N and 60°S latitudes. The global averaging operator ($\bar{\quad}$) used in subsection 2.1 and 2.2 indicates area averaging of (\quad) over this domain, which covers 87% of the globe.

3. Annual Variation of Cloud Forcing

3.1. Annually Normalized Solar Cloud Forcing

In Figure 2a, the global mean annually normalized solar cloud forcing ($\overline{CF_{SA}}$) is plotted against the global mean surface temperature ($\overline{T_s}$) for 12 months. The correlation between the two variables is not significantly different from zero (confidence level = 95%). The solar cloud gain factor (f_{CS}) is computed using (16). The regression coefficient between the annually normalized solar cloud forcing and the global mean surface temperature is $+0.139 \text{ W m}^{-2} \text{ K}^{-1}$, yielding small positive value of f_{CS} , i.e., $+0.042$. This value, the relative magnitude of feedback effect to basic negative blackbody radiative feedback, is much smaller than 1. The present result implies that on a global scale, solar cloud forcing exerts hardly any feedback upon the annual variation of the global mean surface temperature.

In order to investigate how the global mean cloud reflectivity depends upon the annual variation of global mean surface temperature, we obtain the annually normalized solar cloud forcing per unit cloudy area, dividing the global mean, annually normalized solar cloud forcing by globally averaged total cloudiness ($\overline{C_T}$). This quantity is negative, representing the loss of energy from the top of the atmosphere due to the reflection of solar energy from unit cloudy area. Reversing its sign, it is proportional to the cloud reflectivity of solar radiation at the top of the atmosphere (i.e., the planetary

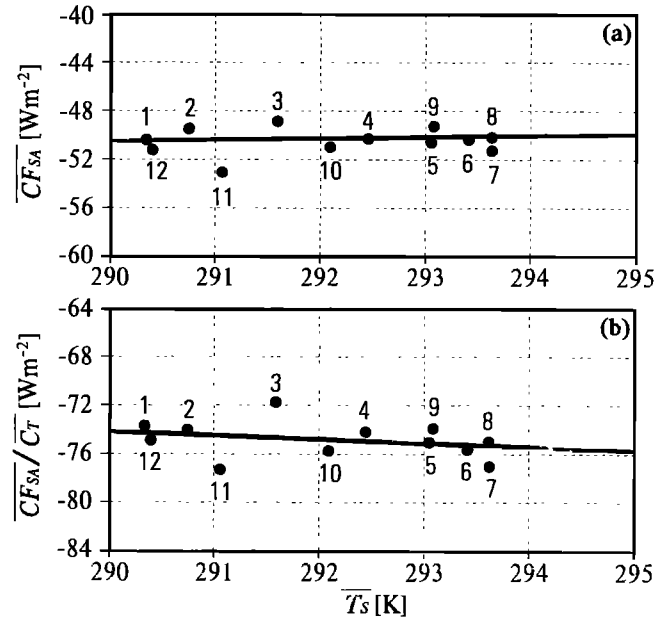


Figure 2. For each month, globally averaged monthly mean values of (a) annually normalized solar cloud forcing ($\overline{CF_{SA}}$ (W m^{-2})) and (b) annually normalized solar cloud forcing per unit cloudy area ($\overline{CF_{SA}/C_T}$ (W m^{-2})) are plotted against the global mean surface temperature ($\overline{T_s}$ (K)). The number near each dot indicates the month plotted. The slopes of the regression lines in Figures 2a and 2b are 0.14 and -0.32 , respectively.

albedo of clouds). The 12 monthly values of this variable are plotted in Figure 2b against the global mean surface temperature. Figure 2b indicates that the annually normalized cloud forcing per unit cloudy area does not depend systematically upon the global mean surface temperature because neither globally averaged annually normalized solar cloud forcing (Figure 2) nor total cloudiness (Figure 3) depend significantly upon the global mean surface temperature. In short, global mean planetary albedo of cloud cover does not depend significantly upon global mean surface temperature.

As noted earlier, cloud optical thickness is a crude indicator of cloud reflectivity of visible radiative flux. Rossow and Lacis [1990] analyzed the relationship between global mean cloud optical thickness and the global mean surface temperature. They found that global mean cloud optical thickness shows little dependence on the global mean surface temperature.

Here we have conducted similar analysis using the data of ISCCP, obtained from geostationary weather satellites. The data, which were compiled by Rossow and Schiffer [1991], have better temporal resolution (8 times per day) and cover longer periods (about 6 years) than the data used by Rossow and Lacis [1990]. The global mean optical thickness ($\overline{\tau}$) was computed for 12 months using the level D2 data and are plotted in Figure 4 against the global mean surface temperature. Again, the correlation between the two variables is not significantly different from zero (confidence level = 95%), confirming the earlier finding of Rossow and

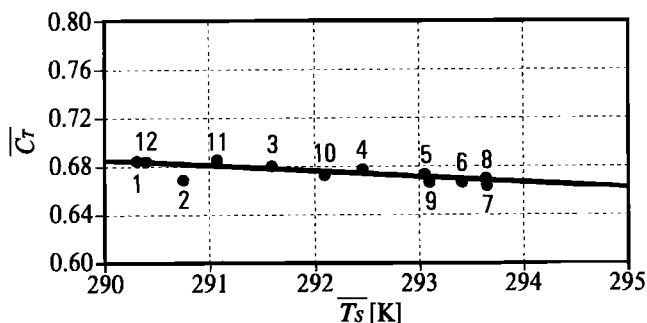


Figure 3. As previous figures but plotting globally averaged monthly mean total cloudiness ($\overline{C_T}$) against the global mean surface temperature ($\overline{T_s}$ (K)). The slope of the regression line is -0.0047 .

Lacis [1990] that global mean cloud optical thickness does not depend upon temperature.

3.2. Longwave Cloud Forcing

Figure 5a shows the scatter plot of global mean longwave cloud forcing ($\overline{CF_L}$) versus the global mean surface temperature. The correlation between the two variables is not significantly different from zero (confidence level = 95%). Cloud gain factor (f_{CL}) is computed from the slope of the regression line to be -0.083 . *Inamdar and Ramanathan* [1998], in their study of global scale water vapor feedback, also noted that cloud longwave forcing feedback does not contribute to the global sensitivity. Although it is just a comment without quantitative discussion, their result appears to be consistent with what we obtained here.

In order to evaluate the effect of cloud height change upon the longwave components of the cloud feedback process, we divided global mean longwave cloud forcing by total cloudiness, which decreases slightly with increasing global mean surface temperature, as shown in Figure 3. The global mean longwave cloud forcing per unit cloudy area thus computed is plotted against the global mean surface temperature in Figure 5b. Again the correlation between the two variables is not significantly different from zero (confidence level = 95%), indicating that the effective emission temperature of cloud for outgoing longwave radiation, on a global scale,

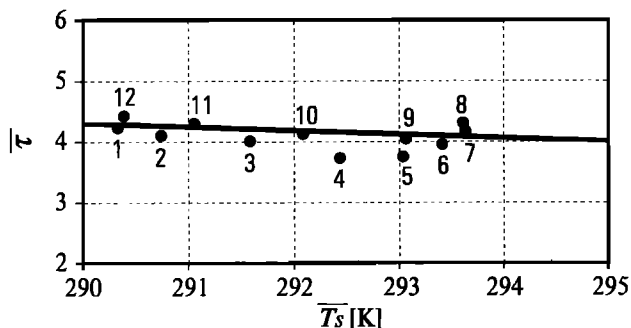


Figure 4. As previous figures but plotting globally averaged monthly mean cloud optical thickness ($\overline{\tau}$) against the global mean surface temperature ($\overline{T_s}$ (K)). The slope of the regression line is -0.06 .

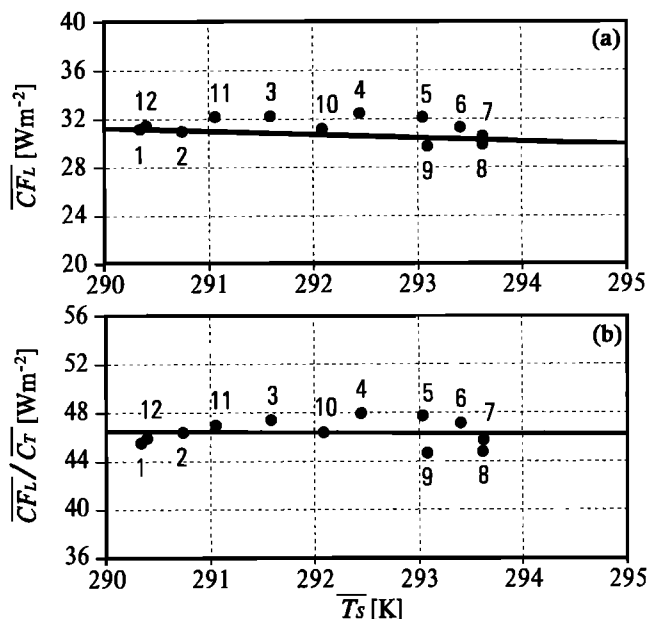


Figure 5. As previous figures but plotting (a) longwave cloud forcing ($\overline{CF_L}$ (W m^{-2})) and (b) longwave cloud forcing per unit cloudy area ($\overline{CF_L}/\overline{C_T}$ (W m^{-2})) against the global mean surface temperature ($\overline{T_s}$ (K)). The slopes of the regression lines in Figures 5a and 5b are -0.28 and -0.09 , respectively.

shows little dependence on the global mean surface temperature. This result implies that on a global scale, cloud effective height does not depend significantly upon surface temperature.

Determining cloud height from the data of 11 micron radiance, which were obtained by NOAA 5 Scanning Radiometer data, *Rossow and Lacis* [1990] demonstrated that the annual variation of global mean cloud height shows little dependence on that of the global mean surface temperature. Their conclusion appears to be consistent with the present results.

Here we have performed similar analysis using IS-CCP D2 data compiled by *Rossow and Schiffer* [1991]. Monthly mean cloud top temperature obtained by IS-CCP is converted to the physical height, using height field data of NCEP/NCAR reanalysis [*Kalnay et al.*, 1996]. Global mean cloud top height thus obtained is plotted against the global mean surface temperature for 12 months as shown in Figure 6. The correlation between the two variables is not significantly different from zero (confidence level = 95%), indicating that global mean cloud height has little dependence on the global mean surface temperature. Both the present and earlier analysis of *Rossow and Lacis* [1990] are consistent with the analysis of longwave cloud forcing conducted here.

3.3. Annually Normalized Total Cloud Forcing

In this subsection, we analyze annually normalized total cloud forcing $\overline{CF_A}$, which is the sum of annually normalized solar cloud forcing and longwave cloud forcing ($\overline{CF_A} = \overline{CF_{SA}} + \overline{CF_L}$). In Figure 7a, annually nor-

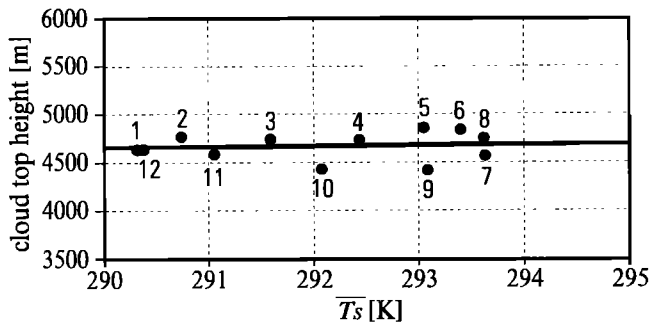


Figure 6. As previous figures but plotting globally averaged monthly mean cloud top height (m) against the global mean surface temperature (\bar{T}_s (K)). The slope of the regression line is 8.99.

malized total cloud forcing is plotted against the global mean surface temperature for 12 months. Again the correlation between the two variables is not significantly different from zero (confidence level = 95%). Cloud gain factor f_C ($= f_{CS} + f_{CL}$) is computed from the regression coefficient, yielding -0.041 . This result indicates that the cloud feedback process as a whole neither reduces nor enhances the annual variation of the global mean surface temperature.

Dividing the global mean annually normalized total cloud forcing by total cloudiness, we computed the annually normalized total cloud forcing per unit cloudy area. The 12 monthly values of this variable are plotted against the global mean surface temperature as shown in Figure 7b. This figure shows that the annually normalized total cloud forcing per unit cloud-covered area does not depend significantly upon the global mean surface temperature. It appears that cloud radiative forcing does not significantly affect the annual variation of the global mean surface temperature on a global scale.

4. Comparison With Models

One of the most challenging tasks in modeling the cloud feedback process is the parameterization of the microphysical properties of cloud cover. Among the atmospheric models submitted to the Atmospheric Model Intercomparison Project I (AMIP I) [Gates, 1992], we chose three atmospheric GCMs, in which the microphysical properties of cloud cover are predicted explicitly. Fortunately, for these three models, AMIP data bank contains the information on solar and longwave cloud forcing separately, making it possible to compute cloud gain factors in a manner similar to the analysis of ERBE data described in section 3.

The cloud gain factors of the three models are tabulated in Table 1. For comparison, those computed from observed cloud forcing are added to the same table. This table indicates that cloud gain factor f_C is -0.020 for Center for Climate System Research/National Institute for Environmental Study (CCSR/NIES) and $+0.024$ for United Kingdom Meteorological Office (UKMO) models and is small in qualitative agreement

with observations. However, when one looks separately at solar and longwave gain factors (i.e., f_{CS} and f_{CL}), they are not necessarily small for CCSR/NIES and Max Planck Institute for Meteorology (MPI) models (though they are small for the UKMO model).

Solar and longwave cloud forcing are affected by not only cloud optical properties but also cloudiness. Here we examine how these cloud forcings per unit cloud-covered area in these models are affected by the global mean surface temperature. From such analysis, we found the systematic differences between model simulations and observation described below.

In Figure 8, globally averaged monthly mean total cloudiness is plotted against the global mean surface temperature. In all three models, total cloudiness decreases slightly with increasing temperature, in qualitative agreement with observation (see Figure 8d). The slopes of the regression, however, are larger than the observation.

To determine how solar reflectivity of clouds depends upon the surface temperature, we divided the monthly mean value of globally averaged, annually normalized solar cloud forcing by total cloudiness and plotted it against the global mean surface temperature in Figure 9. In all three models, the annually normalized solar cloud forcing per unit cloudy area thus computed increases substantially with increasing surface temperature. This is in sharp contrast to observations in which the former shows little dependence on the latter (Figure 9d). The results shown here imply that the solar reflectivity of clouds increases sharply with increasing surface temperature in all three models.

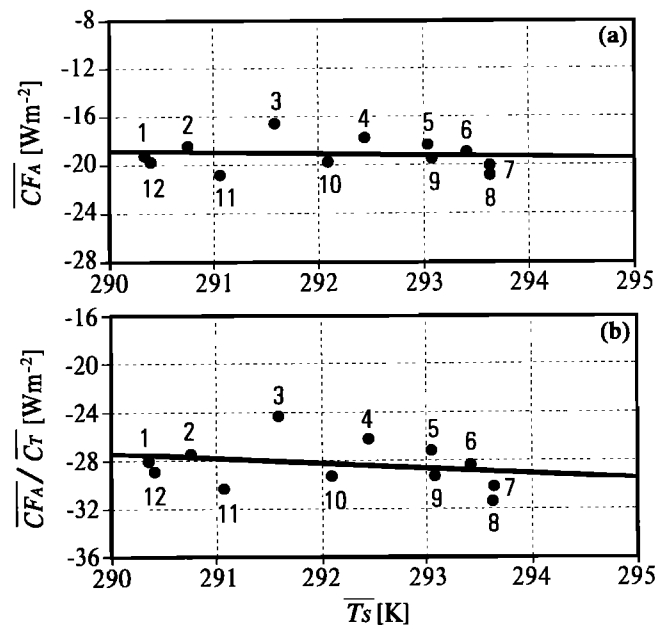


Figure 7. As previous figures but plotting (a) annually normalized total cloud forcing (\overline{CF}_A (W m^{-2})) and (b) annually normalized total cloud forcing per unit cloudy area ($\overline{CF}_A/\overline{C_T}$ (W m^{-2})) against the global mean surface temperature (\bar{T}_s (K)). The slopes of the regression lines in Figures 7a and 7b are -0.14 and -0.41 , respectively.

Table 1. The f_{CS}, f_{CL}, f_C and related variables in GCM With Prognostic Cloud Scheme^a

	$\frac{dCF_{SA}}{dT_s}$ ($W m^{-2}$)	$\frac{dCF_L}{dT_s}$ ($W m^{-2}$)	$f_{C,S}$	$f_{C,L}$	f_C
CCSR/NIES	-0.496	+0.432	-0.150	+0.131	-0.020
MPI	-0.697	+0.350	-0.211	+0.106	-0.105
UKMO	-0.052	+0.131	-0.016	+0.040	+0.024
ERBE	+0.139	-0.275	+0.042	-0.083	-0.041

^aObservational values are listed at the bottom for reference.

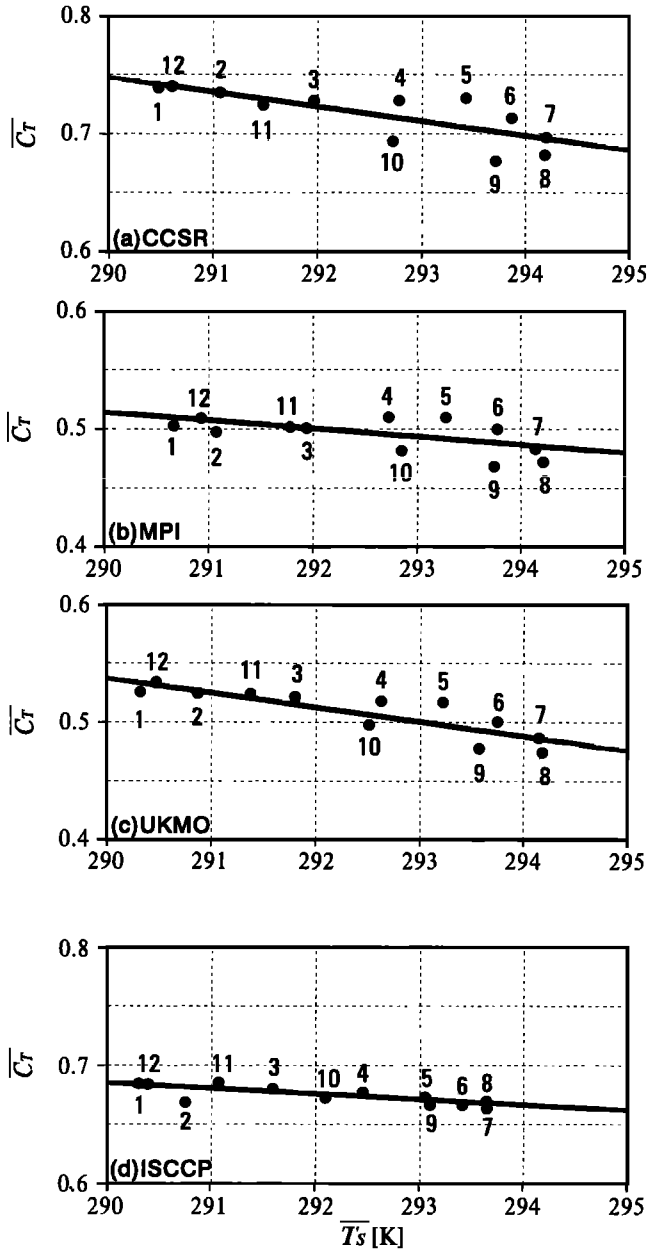


Figure 8. As previous figures but plotting globally averaged monthly mean total cloudiness ($\overline{C_T}$) against the global mean surface temperature ($\overline{T_s}$ (K)) in (a) CCSR/NIES, (b) MPI, and (c) UKMO. (d) For comparison, that computed from observed data is added in the bottom row. The slopes of the regression lines in Figures 8a, 8b, 8c, and 8d are -0.0124 , -0.0068 , -0.0123 , and -0.047 , respectively.

In order to explore why global mean solar cloud reflectivity increases with global mean surface temperature in the CCSR/NIES model, we computed the global mean cloud water content of the model, dividing the globally integrated weight of cloud water by that of cloud-containing air mass. The monthly mean value of global mean cloud water content thus computed is plotted against that of global mean surface temperature in Figure 10. This figure indicates that the global mean cloud water content increases significantly with increasing global mean surface temperature. As the global mean surface temperature increases from January to July for example, the percentage increase in global mean cloud water content during the same period (Figure 10) is comparable to the percentage change in annually normalized solar cloud forcing (Figure 9a). (Note that the absolute value of annually normalized solar cloud forcing is proportional to the planetary cloud albedo.) The result presented here implies that, at least for the CCSR model, the dependence of global mean planetary cloud albedo upon the global mean surface temperature is attributable, in no small part, to the change in global mean cloud water content.

To determine how the effective temperature for outgoing radiation depends upon surface temperature, globally averaged monthly mean longwave cloud forcing is divided by total cloudiness and is plotted against the global mean surface temperature (Figure 11). This figure indicates that longwave cloud forcing per unit cloudy area increases substantially with increasing surface temperature in all three models, in sharp contrast to observation in which longwave cloud forcing per unit cloudy area shows little dependence on surface temperature (see Figure 11d). This result implies that the effective temperature, and accordingly, the effective height of cloud top for outgoing radiation, on a global scale, increase significantly with increasing surface temperature in all three models.

The increase of the effective temperature for the outgoing radiation described above may, at least partly, be attributable to the increase of mean cloud height with increasing temperature. To evaluate this speculation, the global mean cloud height weighted by cloud water is computed for the CCSR/NIES model and is

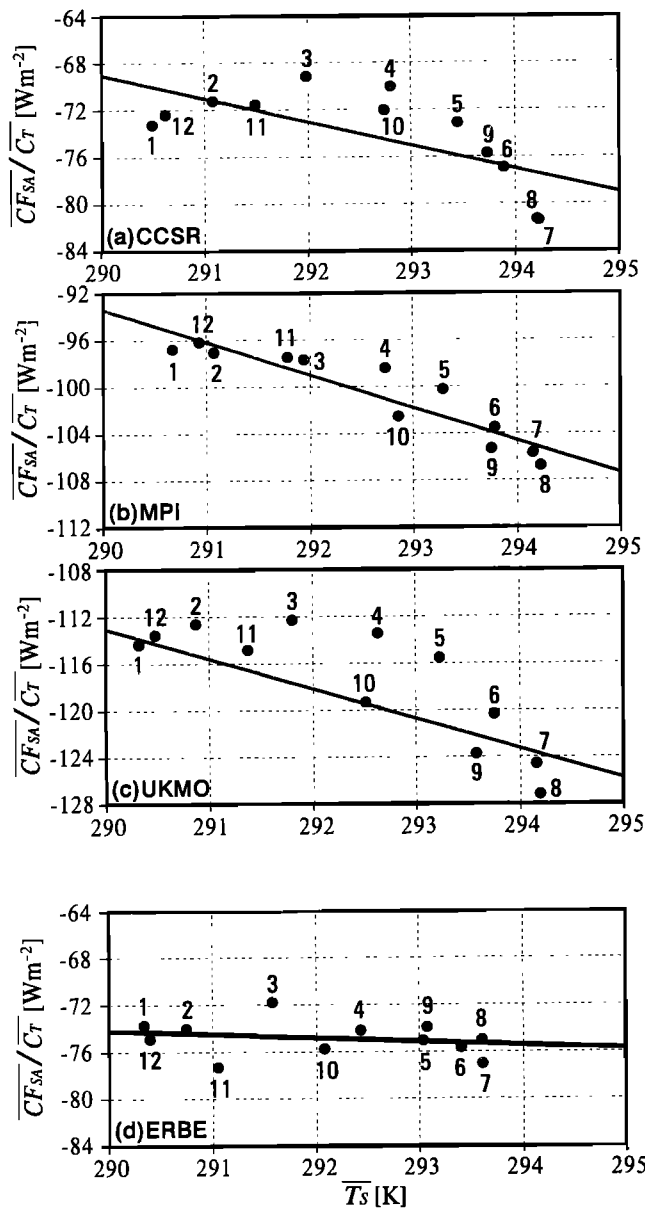


Figure 9. As previous figures but plotting annually normalized solar cloud forcing per unit cloudy area (CF_{SA}/C_T ($W m^{-2}$)) against global mean surface temperature (\bar{T}_s (K)) in (a) CCSR/NIES, (b) MPI, and (c) UKMO. (d) For comparison, that computed from observed data is added in the bottom row. The slopes of the regression lines in Figures 9a, 9b, 9c, and 9d are -2.01 , -2.82 , -3.00 , and -0.32 , respectively.

plotted against the global mean surface temperature in Figure 12. This figure indicates that mean cloud height increases significantly with increasing temperature, on a global scale, which supports the above-mentioned speculation.

5. Summary and Conclusions

This study investigated the influence of cloud feedback process upon the annual variation of the global mean surface temperature, using the radiative flux data from the Earth Radiation Budget Experiment. We

found that both global mean annually normalized solar cloud forcing and longwave cloud forcing depend little upon the annual variation of global mean surface temperature. Thus clouds neither amplify nor damp the annual variation of global mean surface temperature. The analysis of solar radiative forcing and optical properties of cloud indicates that not only the reflectivity but also the amount and effective height of cloud depend very little upon global mean surface temperature. In short, cloud feedback hardly affects the annual variation of surface temperature on a global scale.

On the basis of the results summarized above, one is tempted to speculate that cloud feedback has little effect on the annual variation of global mean temperature or on global warming. However, such speculation is premature in view of the large difference in the pattern of temperature change between the two phenomena.

Using the analysis of aircraft observations over Russia, *Feigelson* [1978] noted that liquid water content of stratus clouds increases with increasing temperature, thereby increasing its reflectivity of solar radiation. Referring to the results of her study, *Somerville and Remer* [1984] speculated that, in general, the albedo of clouds may increase with increasing temperature, exerting negative feedback upon the climate. Using ISCCP data from geostationary satellites, *Tselioudis et al.* [1992] determined the optical thickness of clouds, which may be regarded as a crude indicator of cloud reflectivity. Their results indicate that, although the optical thickness of clouds increases with increasing temperature in high latitudes, it decreases in the tropical and subtropical latitudes. Obviously, both the microphysical properties and the distribution and type of cloud undergo large seasonal variations. Therefore it is premature to judge the validity of the speculation of Somerville and Remer based upon the feedback analysis of simulated and observed annual variation. Nevertheless, our result suggests that global mean planetary cloud albedo does not increase with increasing global mean surface temperature, apparent contradicting the speculation of Somerville and Remer.

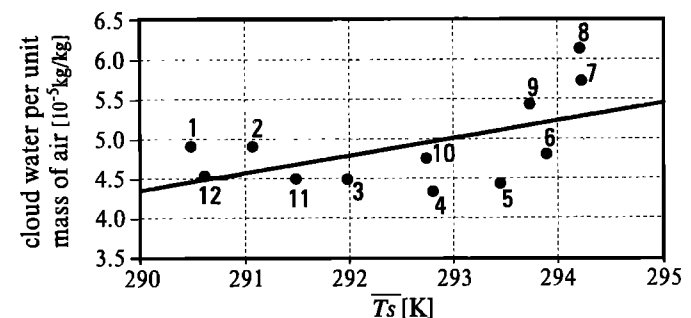


Figure 10. As previous figures but plotting globally averaged monthly mean cloud water content per unit cloud-containing air mass ($10^{-5} kg kg^{-1}$) of the CCSR/NIES GCM is plotted against the global mean surface temperature (\bar{T}_s (K)). The slope of the regression line is $2.20 \times 10^{-6} (kg kg^{-1} K^{-1})$.

In the annual variation of the three AMIP models, in which the microphysical properties of clouds are predicted explicitly, the globally averaged planetary cloud albedo increases with increasing global mean surface temperature. The analysis of one model, for which cloud water information is available to us, indicates that the global mean cloud water content also increases with global mean surface temperature in conformity with the speculation made by Somerville and Remer. It is found that both global mean annually normalized solar cloud forcing and longwave cloud forcing depend little upon the annual variation of global mean surface temperature. Thus clouds neither amplify nor damp the an-

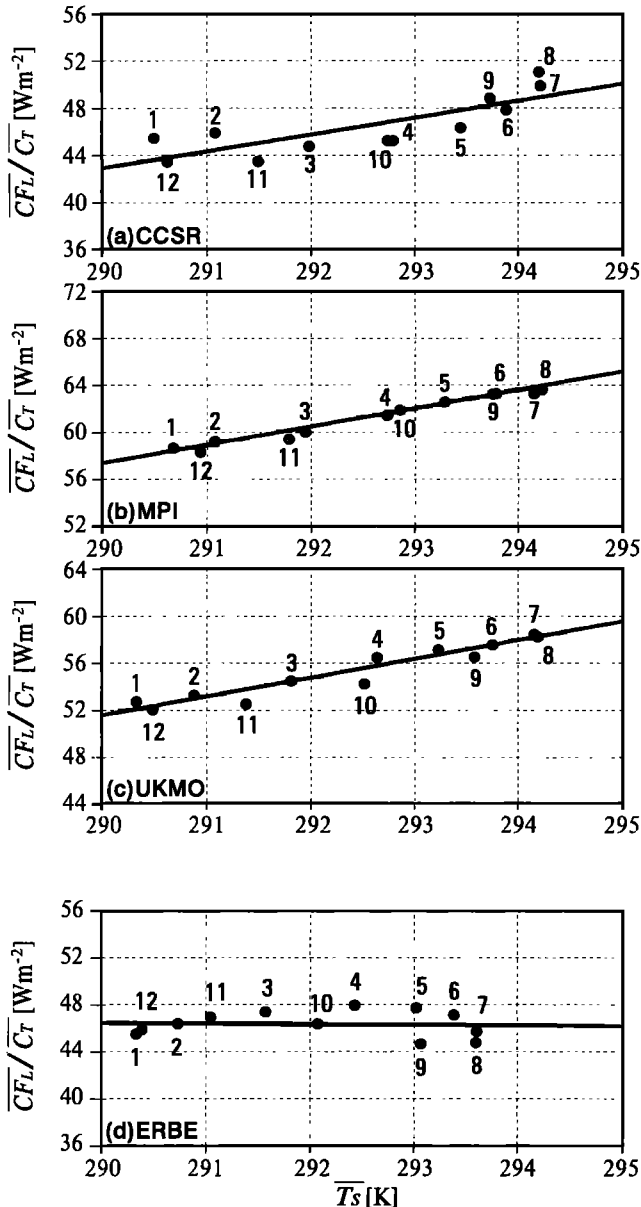


Figure 11. As previous figures but plotting longwave cloud forcing per unit cloud area ($\overline{CF_L}/\overline{C_T}$ (W m^{-2})) against global mean surface temperature ($\overline{T_s}$ (K)) in (a) CCSR/NIES, (b) MPI, and (c) UKMO. (d) For comparison, that computed from observed data is added in the bottom row. The slopes of the regression lines in Figures 11a, 11b, 11c, and 11d are 1.42, 1.55, 1.59, and -0.09 , respectively.

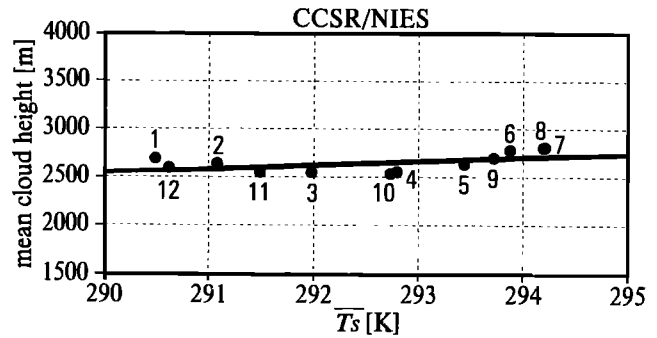


Figure 12. As previous figures but plotting globally averaged monthly mean cloud height (m) weighted by cloud water against the global mean surface temperature ($\overline{T_s}$ (K)) in CCSR/NIES GCM. The slope of the regression line is 42.46.

nual variation of global mean surface temperature. The analysis of solar radiative forcing and optical properties of clouds indicates that not only the reflectivity but also the amount and effective height of cloud depends very little upon global mean surface temperature. In short, cloud feedback process hardly affects the annual variation of surface temperature at global scale. The result presented here suggests that the parameterization of microphysical properties of cloud in these three models may be biased systematically as compared with observation.

We also found that globally averaged effective cloud top height, which is determined from the analysis of observed outgoing longwave radiation at the top of the atmosphere, hardly changes despite the annual variation of the global mean surface temperature. In contrast, global mean cloud top height increases significantly with increasing global mean surface temperature in all three models selected for the present analysis. In the numerical experiments conducted earlier by *Wetherald and Manabe* [1988] and *Senior and Mitchell* [1993], the altitude of high clouds also increases in response to the increase in atmospheric CO_2 concentration. The increase in cloud top height helps reduce the effective emission temperature for the outgoing radiation from the top of the atmosphere, enhancing CO_2 -induced warming. In interpreting of the above results, one has to recognize, however, that the seasonal changes in the distribution and type of cloud are much larger and are quite different from the change associated with simulated CO_2 -induced warming. Nevertheless, the present study suggests that some current models may exaggerate the positive feedback effect, which involves the change in cloud altitude.

Comparing the observed and simulated strength of the cloud feedback process that operates on the annual variation of global mean surface temperature, one can identify the systematic bias of a model. Therefore we would like to recommend the comparative analysis of observed and simulated cloud feedback processes in the annual variation of global mean surface temperature as an effective test for evaluating models.

Appendix A

In order to estimate cloud gain factors from solar and longwave cloud forcing using (25), we ignore the contributions of the changes in temperature, water vapor, and surface albedo to the total derivative cloud forcing with respect to the global mean surface temperature (i.e., the second and third terms of (20) and (21)). We attempted to estimate the order of magnitude of these terms, using FSTAR5C of the general package R-Star in the System for Transfer of Atmospheric radiation series, developed at the University of Tokyo and Munich University. The R-Star package is based upon the algorithm of *Nakajima and Tanaka* [1983, 1986, 1988], and a LOWTRAN 7 gas absorption model [Kneizys *et al.*, 1986]. Instead of a realistic distribution, we assumed an idealized distribution of cloud cover, which is uniform horizontally and does not change with season. Low, middle, high and deep convective clouds are placed at the altitudes of 2, 5, 10, and 2 km-10 km and have cloud fractions of 0.275, 0.190, 0.026, and 0.196, respectively. The cloud amounts are determined subjectively referring to the study of *Rossow and Shiffer* [1999] and are adjusted such that they yield more or less realistic global mean cloud forcing (i.e. -50 and -30 W m^{-2} for solar and longwave cloud forcing, respectively).

We next estimate the second and the third term on the right-hand side of (20), i.e., the effect of the changes in water vapor and surface albedo associated with the unit annual change in the global mean surface temperature. Considering the latitudinal dependency of surface albedo and water vapor distribution, we calculated the contributions from the seven latitude belts, i.e., 60°S - 52.5°S , 52.5°S - 45°S , 45°S - 30°S , 30°S - 30°N , 30°N - 45°N , 45°N - 52.5°N , and 52.5°N - 60°N . Globally averaged, annually normalized solar cloud forcing is obtained from the weighted average of the contributions from the seven latitude belts identified above.

First we estimated how the annually normalized solar cloud forcing is affected by the annual change in water vapor content of the atmosphere. As surface temperature changes, the temperature profile of the U.S. standard atmosphere is shifted in parallel with the original profile, keeping the vertical profile of relative humidity unchanged. Assuming that all other relevant variables remain unchanged, the calculation shows that the annually normalized solar cloud forcing changes as little as -0.004 $\text{W m}^{-2} \text{K}^{-1}$ in response to the change in water vapor associated with a unit change in surface temperature. This translates into an inaccuracy of solar cloud gain factor of -0.001 , which is extremely small.

Second we estimated the third term of (20), i.e., the change in annually normalized solar cloud forcing in response to the change in the surface albedo associated with a unit annual change in the global mean surface temperature. Annually normalized solar cloud forcing is calculated over the surface albedos in two months (January and July), assuming the idealized cloud dis-

tribution described earlier as well as all other relevant variables remaining unchanged. We referred to the International Satellite Land Surface Climatology Project (ISLCP) [Sellers *et al.*, 1995] for seven latitudinal mean surface albedos. The calculation shows that annually normalized solar cloud forcing increases by 0.24 W m^{-2} with 1 K annual change in the global mean surface temperature. This leads to an inaccuracy in the solar cloud gain factor of 0.073 , which is not negligible but small.

We also estimate the sum of the second and third terms on the right-hand side of (21), i.e., the combined effect of the changes in temperature and water vapor per unit change in the global mean surface temperature. For this purpose, we estimated the change in longwave cloud forcing when the temperature profile is offset so that it remains the original profile, keeping the vertical profile of relative humidity unchanged. Assuming that the idealized cloud cover as well as all other relevant variables remain unchanged, the calculation shows that longwave cloud forcing increases by 0.072 W m^{-2} in response to a 1 K change in temperature and associated change in water vapor. This results in a inaccuracy in the longwave cloud gain factor of 0.022 and is small.

In conclusion, the magnitudes of the second and third terms in (20) and (21) appear to be small. Therefore one can assume that the approximate (25) holds, justifying the computation of cloud gain factors from satellite observation of solar and longwave radiative forcing.

Acknowledgments. We are grateful to G. L. Potter of the AMIP Project Office for providing us AMIP cloud radiative forcing data. D. F. Young of NASA Langley Research Center kindly provided us the information on the accuracy of the ERBE data. T. Nakajima and A. Numaguti gave us much valuable advice. We thank D. L. Hartmann, A. Abeouchi, and K. Sakai for their comments, which have been very useful for improving the manuscript. Finally, we thank T. Mikami for preparing the graphics.

References

- Charlock, T. P., and V. Ramanathan, The albedo field and cloud radiative forcing produced by a general circulation model with internally generated cloud optics, *J. Atmos. Sci.*, **42**, 1408-1429, 1985.
- Dickinson, R. E., Convergence rate and stability of ocean-atmosphere coupling schemes with a zero-dimensional climate model, *J. Atmos. Sci.*, **38**, 2112-2120, 1981.
- Feigelson, E. M., Preliminary radiation model of a cloudy atmosphere, 1, Structure of clouds and solar radiation, *Beitr. Phys. Atmos.*, **51**, 203-229, 1978.
- Gates, W. L., AMIP: The Atmospheric Model Intercomparison Project, *Bull. Am. Meteorol. Soc.*, **73**, 1962-1970, 1992.
- Hansen, J, A. Lacis, D. Rind, G. Russell, P. Stone, I. Fung, R. Ruedy, and J. Lerner, Climate sensitivity: Analysis of feedback mechanisms in *Climate Process and Climate Sensitivity*, edited by J. Hansen and T. Takahashi, *Geophys. Monogr. Ser.*, vol. 29, pp. 130-163, AGU, Washington, D. C., 1984.
- Harrison, E. F., P. Minnis, B. R. Barkstrom, V. Ramanathan, R.D. Cess, and G. G. Gibson, Seasonal variation of cloud radiative forcing derived from the Earth Ra-

- diation Budget Experiment, *J. Geophys. Res.*, *95*, 18,687-18,703, 1990.
- Inamdar, A. K., and V. Ramanathan, Tropical and global scale interactions among water vapor, atmospheric greenhouse effect, and surface temperature, *J. Geophys. Res.*, *103*, 32,177-32,194, 1998.
- Kalnay, E., et al., The NCEP/NCAR 40-Year reanalysis project, *Bull. Am. Meteorol. Soc.*, *77*, 437-471, 1996.
- Kneizys, F. X., E. P. Shettle, L. W. Abreu, J. H. Chetwynd, G. P. Anderson, W. O. Gallery, J. E. A. Selby and S. A. Clough, Users guide to LOWTRAN 7, *Rep. AFGL-TR-88-0177*, Air Force Geophys. Lab., Hanscom AFB, Mass, 1986.
- Nakajima, T., and M. Tanaka, Effect of wind-generated waves on the transfer of solar radiation in the atmosphere-ocean system, *J. Quant. Spectrosc. Radiat. Transfer*, *29*, 521-537, 1983.
- Nakajima, T., and M. Tanaka, Matrix formulations for the transfer of solar radiation in a plane-parallel scattering atmosphere, *J. Quant. Spectrosc. Radiat. Transfer*, *35*, 13-21, 1986.
- Nakajima, T., and M. Tanaka, Algorithms for radiative intensity calculations in moderately thick atmospheres using a truncation approximation, *J. Quant. Spectrosc. Radiat. Transfer*, *40*, 51-69, 1988.
- Manabe, S., and R. Wetherald, Thermal equilibrium of the atmosphere with a given distribution of relative humidity, *J. Atmos. Sci.*, *24*, 241-259, 1967.
- Nemesure, S., R. D. Cess, E. G. Dutton, J. J. Deluisi, Z. Li, and H. G. Leighton, Impact of cloud on the short-wave radiation budget of the surface-atmosphere System for snow-covered surfaces, *J. Clim.*, *4*, 579-585, 1994.
- Ramanathan, V., R. D. Cess, E. F. Harrison, P. Minnis, B. R. Barkstrom, E. Ahmad, D. Hartmann, Cloud-radiative forcing and climate: Results from the Earth Radiation Budget Experiment, *Science*, *243*, 57-63, 1989.
- Rossow, W. B., and A. A. Lacis, Global, seasonal cloud variations from satellite radiance measurements. Part II: Cloud properties and radiative effects, *J. Clim.*, *3*, 1204-1253, 1990.
- Rossow, W. B., and R. A. Schiffer, ISCCP cloud data products., *Bull. Am. Meteorol. Soc.*, *72*, 2-20, 1991.
- Rossow, W. B., and R. A. Schiffer, Advances in understanding clouds from ISCCP, *Bull. Am. Meteorol. Soc.*, *80*, 2261-2287, 1999.
- Sellers, P. J., et al., Remote sensing of the land surface for studies of global change: Models - algorithms - experiments, *Remote Sens. Environ.*, *51*, 3-26, 1995.
- Senior, C. A., and J. F. B. Mitchell, Carbon dioxide and climate: The impact of cloud parameterization, *J. Clim.*, *6*, 393-418, 1993.
- Somerville, R. C. J., and L. A. Remer, Cloud optical thickness feedbacks in the CO₂ climate problem, *J. Geophys. Res.*, *89*, 9668-9672, 1984.
- Tselioudis, G., W. B. Rossow, and D. Rind, Global patterns of cloud optical thickness variation with temperature, *J. Clim.*, *5*, 1484-1495, 1992.
- Wetherald, R. T., and S. Manabe, Cloud feedback process in a general circulation model, *J. Atmos. Sci.*, *45*, 1397-1415, 1988.

S. Manabe and Y. Tsushima, Frontier Research System for Global Change, 3173-25 Showamachi, Kanazawa-ku, Yokohama City, Kanagawa 236-0001, Japan. (e-mail: tsussi@jamstec.go.jp)

(Received December 7, 2000; revised May 24, 2001; accepted June 7, 2001.)